The effect of inlet constriction on bubble growth during flow boiling in microchannels

A. Mukherjee [a,*], S.G. Kandlikar [b]

[a] Department of Mechanical Engineering and Engineering Mechanics, Michigan Technological University, 1400 Townsend Drive, Houghton, MI 49931, USA
[b] Department of Mechanical Engineering, Rochester Institute of Technology, 76, Lomb Memorial Drive, Rochester, NY 14623, USA

ABSTRACT

Flow boiling through microchannels is characterized by nucleation of vapor bubbles on the channel walls. In parallel microchannels connected through a common header, formation of vapor bubbles often results in flow mal-distribution that leads to reversed flow in certain channels. One way of eliminating the reversed flow is to incorporate flow restrictions at the channel inlet. In the present study, a nucleating vapor bubble placed near the restricted end of a single microchannel is numerically simulated. Placing restrictions at channel inlet increased the incoming liquid velocity for the same flow rate that prevented explosive bubble growth and reversed flow. It is proposed that channels with increasing cross-sectional area may be used to promote unidirectional growth of the vapor plugs and prevent reversed flow.

© 2009 Elsevier Ltd. All rights reserved.

1. Introduction

Flow boiling in microchannels can result in very high wall heat transfer coefficients. However, when the hydraulic diameter of a channel is decreased, the pressure drop increases for the same flow velocity. The small cross-sectional area of the microchannels gets easily filled by nucleating vapor bubbles and soon the vapor bubbles turn into elongated bubbles or vapor plugs. The surface area available for vapor addition into the plug increases directly with increase in length of the plug. This causes the vapor plug interfaces normal to the flow direction to accelerate causing high pressure gradients inside the channels. In parallel microchannels connected with common headers, random temporal and spatial bubble nucleation in the channels cause flow mal-distribution leading to reversed flow. The liquid in the inlet header tries to flow into the channels least blocked by vapor bubbles. The reversed flow is detrimental to the heat transfer and leads to early CHF condition.

It has been experimentally observed by Balasubramanian and Kandlikar [1] that in some of the parallel microchannels, the upstream interface of the vapor plug moves towards the inlet. Fig. 1 shows high speed images of reversed flow in parallel channels as obtained by them.

The above phenomenon could occur due to two reasons as explained in Fig. 2. The rate of vapor generation at the upstream interface can be more than the rate of liquid supply to the channel from the inlet header (Fig. 2(a)) causing the interface to move to-

wards the inlet. Otherwise the vapor plug growth may be too rapid to cause high pressure buildup near the upstream interface pushing the liquid back into the inlet header (Fig. 2(b)).

The first situation can be avoided by ensuring sufficient inflow of liquid corresponding to the wall heat flux conditions. The means to avoid the second scenario is being addressed in this paper.

2. Literature review

Hetsroni et al. [2] investigated flow instability in uniformly heated triangular microchannels. The growth and collapse of vapor fraction were found to cause fluctuations in pressure drop and decreased the heat transfer coefficient. The maximum values of pressure fluctuations were found to be in the order of the pressure drop across the channels.

Peles [3] studied two-phase boiling in micro heat exchanger consisting of 16 mm long multiple parallel triangular microchannels with hydraulic diameter ranging from 50 μm to 200 μm. He observed a 'rapid bubble flow' regime where the vapor bubble accelerated inside the channel after filling up the channel cross-section.

Wu and Cheng [4] carried out flow boiling experiments in parallel trapezoidal microchannels. They observed large amplitude periodic oscillations during alternate single and two-phase liquid flow. These fluctuations were dependent on channel size, heat flux and mass flux.

Li and Cheng [5] studied boiling incipience in a microchannel using experimental and numerical techniques. Nucleation temperature was found to be dependent on contact angle and presence of dissolved gas. Larger flow rates were found to suppress bubble generation in the microchannel.

* Corresponding author. Tel.: +1 906 487 1174; fax: +1 906 487 2822.
E-mail addresses: mukherje@mtu.edu (A. Mukherjee), sgkeme@rit.edu (S.G. Kandlikar).

Nomenclature

C_p	specific heat at constant pressure		z	distance in z direction
D	bubble diameter		β_T	coefficient of thermal expansion
g	gravity vector		κ	interfacial curvature
H	Heaviside function		μ	dynamic viscosity
h	grid spacing		v	kinematic viscosity
h_{fg}	latent heat of evaporation		ρ	density
k	thermal conductivity		σ	surface tension
L	length of bubble		τ	time period
l_0	length scale		ϕ	level set function
m	mass transfer rate at interface		φ	contact angle
ms	milliseconds			
p	pressure		*Subscripts*	
R	area ratio between channel inlet and outlet		evp	evaporation
Re	Reynolds number		in	inlet
r	radius		l	liquid
T	temperature		sat	saturation
ΔT	temperature difference, $T_w - T_{sat}$		v	vapor
t	time		w	wall
t_0	time scale		x	$\partial/\partial x$
u	x direction velocity		y	$\partial/\partial y$
u_0	velocity scale		z	$\partial/\partial z$
v	y direction velocity			
w	z direction velocity		*Superscripts*	
x	distance in x direction		$*$	non-dimensional quantity
y	distance in y direction		$\rightarrow$	vector quantity

Wu and Cheng [6] studied flow boiling instabilities in parallel silicon microchannels with trapezoidal cross-section. Fluctuations in temperature, pressure and mass flux was observed with alternate appearance of single-phase and two-phase flow. The pressure and mass flux fluctuations were out of phase whereas temperature and pressure fluctuations were in phase.

Li and Peterson [7] studied bubble nucleation in a single trapezoidal microchannel using a microscale platinum heater. They observed three distinct flow patterns; bubbly, wavy and annular depending on the mass flow rate. The bubble nucleation temperature was found to be very high on the smooth heater under the forced flow conditions.

Chang and Pan [8] studied flow boiling instability in 15 parallel microchannels under stable and unstable flow conditions. The authors suggested that the magnitude of pressure drop oscillations may be used as an indicator of reversed flow.

Wang et al. [9] studied flow boiling in parallel as well as in a single microchannel. Unstable flow boiling was observed in both cases when the bubbles periodically expanded upstream into the incoming subcooled liquid.

Wang et al. [10] carried out flow boiling experiments in parallel microchannels with three different inlet flow configurations. In the case when the flow entering the microchannels was restricted, the stable flow occurred with little temperature or pressure fluctuations.

Kandlikar et al. [11] experimentally explored different flow regimes during flow boiling of water in parallel minichannels. Experiments were carried out with six parallel channels each with 1 mm hydraulic diameter. The different flow regimes observed were bubbly flow with nucleate boiling, bubbly flow, slug flow, annular/slug flow, annular/slug flow with nucleate boiling and dry out. Large pressure fluctuations were measured in the channels due to boiling phenomenon. In some situations, slug growth was found to occur in the direction counter to bulk flow forcing liquid and vapor back into the inlet manifold.

Steinke and Kandlikar [12] studied flow boiling and pressure drop in parallel flow microchannels. They measured wall heat fluxes and pressure drop in six parallel channels each of hydraulic diameter of 207 μm. A flow reversal was observed where the vapor interface moved in a direction counter to the bulk flow of liquid.

Balasubramanian and Kandlikar [1] studied pressure drop fluctuations and flow instabilities in a set of six parallel rectangular minichannels, each with 333 μm hydraulic diameter. They measured the velocity of the liquid vapor interface associated with
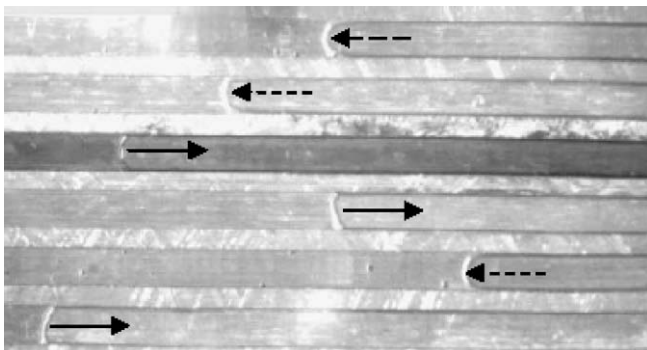

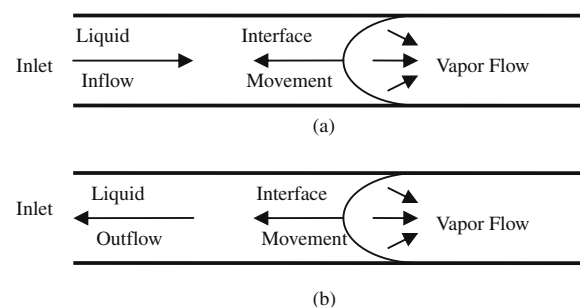**Fig. 1.** Reversed flow in parallel microchannels.

Fig. 2. Schematic representation of liquid flow near the inlet of microchannel with growing vapor bubble.

bubble growth. The bubble/slug growth rate was found to increase with length of the bubble/slug and was as high as 3.5 m/s.

Kandlikar et al. [13] experimentally studied flow boiling through microchannels with pressure drop elements at the inlet. Two different pressure drop elements were used that allowed 51% and 4% open areas. The channels also had artificial nucleation cavities of diameters 5–30 μm. The pressure drop elements of 4% open area completely eliminated the pressure fluctuations and stabilized the flow. However, the total pressure drop increased to a very high value.

All the research work mentioned above were primarily based on experiments. Some researchers have also used analytical or numerical methods to model bubble growth inside small dimension channels. Yuan et al. [14] developed a model of the growth and collapse of a vapor bubble in a small channel connecting two liquid reservoirs. The bubble was assumed to be a sphere from inception until its radius became nearly equal to the tube radius. Thereafter, the bubble was modeled as a cylinder inserted between two hemispheres. The relative velocity between two bubble surface points on the tube axis of the elongated bubble was found to increase or decrease linearly with time. The model showed that the dynamics of the bubble is governed by inertia during most of the bubble lifetime.

Mukherjee and Kandlikar [15] numerically simulated a growing vapor bubble inside a microchannel. The bubble was placed at the center of the channel surrounded by superheated liquid. The bubble length was initially found to increase linearly with time but as the bubble approached the channel wall, the bubble downstream interface was found to accelerate. The bubble growth rate was also found to increase with the incoming liquid superheat.

3. Objective

Bubble/slug expansion inside microchannels leads to rapid rise in liquid pressure around the bubble interfaces. Under extreme conditions, this pressure rise can cause the upstream liquid to flow back towards the inlet header. One possible means to avoid liquid back flow into the inlet header is to provide the inlet with a restriction. The present work is carried out to study vapor bubble growth inside a microchannel during flow boiling with one restricted end. The restrictions at the channels inlets are selected to be the same as used by Kandlikar et al. [13] in their experiments.

4. Numerical model

4.1. Computational domain

Fig. 3 shows the typical computational domain. The domain is $3.96 \times 0.99 \times 0.99$ non-dimensional units in size. Cartesian coordinates have been used with uniform grid.
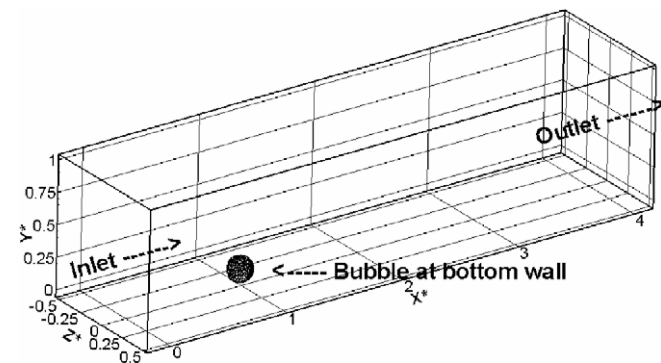

Fig. 3. Computational domain.

When the vapor bubble grows, the liquid leaves the domain at $x^* = 0$ and $x^* = 3.96$. To take advantage of symmetry and reduce computation time, a nucleating cavity is placed on the bottom wall at the center of the microchannel cross-section equidistant from the walls in the x–y planes.

4.2. Grid independence study

The number of computational cells in the domain is $512 \times 128 \times 64$, i.e. 128 grids are used per $0.99l_0$. Different grid sizes used were 80, 96, 112 and 128 to check grid independence. The grid size is chosen to ensure grid independence and negligible volume loss. Variable time step is used which varied typically between 1e−4 to 1e−5 non-dimensional units.

4.3. Method

The entire incompressible Navier–Stokes equations are solved using the SIMPLER method [16], which stands for Semi-Implicit Method for Pressure-Linked Equations Revised. The continuity equation is turned into an equation for the pressure correction. A pressure field is extracted from the known velocity field. After each iteration, the velocities are corrected using velocity-correction formulas. The computations proceed to convergence by the use of a series of continuity satisfying velocity fields. The algebraic equations are solved using the line-by-line technique, which uses TDMA (Tri-Diagonal Matrix Algorithm) as the fundamental unit. The speed of convergence of the line-by-line technique is further improved by supplementing it with the block-correction procedure [17]. The multi-grid method is used to solve the pressure equations.

Sussman et al. [18] introduced a level set approach where the interface was captured implicitly as the zero level set of a smooth function. The level set function was typically a smooth function, designated as ϕ. This formulation eliminated the troubles of adding/subtracting points to a moving grid and automatically took care of merging and breaking of the interface. Furthermore, the level set formulation generalized readily to three dimensions. The current analysis is done using this level set technique.

The liquid vapor interface is identified as the zero level set of a smooth distance function ϕ. The level set function ϕ is negative inside the bubble and positive outside the bubble. The interface is located by solving the level set equation. A fifth order WENO (Weighted, Essentially Non-Oscillatory) scheme is used for left sided and right sided discretization of ϕ [19]. While ϕ is primarily a distance function, it will not remain so after solving the level set equation. Maintaining ϕ as a distance function is vital for providing the interface with a width fixed in time. This is accomplished by reinitialization of ϕ. A modification of Godunov's method is used to decide the upwind directions. The reinitialization equation is solved in fictitious time after each complete time step. With $\Delta\tau = \frac{h}{2u_0}$, ten τ steps are taken with a third order TVD (Total Variation Diminishing) Runge Kutta scheme.

4.4. Governing equations

Momentum equation

$$\rho\left(\frac{\partial \vec{u}}{\partial t} + \vec{u}.\nabla\vec{u}\right) = -\nabla p + \rho\vec{g} - \rho\beta_T(T - T_{sat})\vec{g} - \sigma\kappa\nabla H$$
$$+ \nabla.\mu\nabla\vec{u} + \nabla.\mu\nabla\vec{u}^T \tag{1}$$

Energy equation

$$\rho C_p\left(\frac{\partial T}{\partial t} + \vec{u}.\nabla T\right) = \nabla.k\nabla T \quad \text{for} \quad \phi > 0$$
$$T = T_{sat} \quad \text{for} \quad \phi \leq 0 \tag{2}$$

Continuity equation

$$\nabla.\vec{u} = \frac{\dot{m}}{\rho^2}.\nabla\rho \quad (3)$$

The curvature of the interface

$$\kappa(\phi) = \nabla.\left(\frac{\nabla\phi}{|\nabla\phi|}\right) \quad (4)$$

The mass flux of liquid evaporating at the interface

$$\vec{m} = \frac{k_l \nabla T}{h_{fg}} \quad (5)$$

The vapor velocity at the interface due to evaporation

$$\vec{u}_{evp} = \frac{\vec{m}}{\rho_v} = \frac{k_l \nabla T}{\rho_v h_{fg}} \quad (6)$$

To prevent instabilities at the interface, the density and viscosity are defined as

$$\rho = \rho_v + (\rho_l - \rho_v)H \quad (7)$$
$$\mu = \mu_v + (\mu_l - \mu_v)H \quad (8)$$

H is the Heaviside function given by

$$\begin{aligned} H &= 1 \quad \text{if} \quad \phi \geq +1.5h \\ H &= 0 \quad \text{if} \quad \phi \leq -1.5h \\ H &= 0.5 + \phi/(3h) + \sin[2\pi\phi/(3h)]/(2\pi) \quad \text{if} \quad |\phi| \leq 1.5h \end{aligned} \quad (9)$$

where h is the grid spacing.

Since the vapor is assumed to remain at saturation temperature, the thermal conductivity is given by

$$k = k_l H^{-1} \quad (10)$$

The level set equation is solved as

$$\frac{\partial\phi}{\partial t} + (\vec{u} + \vec{u}_{evp}).\nabla\phi = 0 \quad (11)$$

After every time step, the level set function ϕ, is reinitialized as

$$\frac{\partial\phi}{\partial t} = S(\phi_0)(1 - |\nabla\phi|)u_0 \quad (12)$$
$$\phi(x,0) = \phi_0(x)$$

S is the sign function which is calculated as

$$S(\phi_0) = \frac{\phi_0}{\sqrt{\phi_0^2 + h^2}} \quad (13)$$

4.5. Scaling factors

The governing equations are made non-dimensional using a length scale and a time scale. The length scale l_0 given by the channel width, is equal to 200 μm. If the Reynolds number is specified as 82.4, then for water at 100 °C, the velocity scale u_0 is calculated as 0.12 m/s. The corresponding time scale t_0 is 1.67 ms. All non-dimensional quantities hereafter are indicated with ∗ superscript. The non-dimensional temperature is defined as

$$T^* = \frac{T - T_{sat}}{T_w - T_{sat}} \quad (14)$$

4.6. Initial conditions

A bubble is placed at $x^* = 0.99$, $y^* = 0$ and $z^* = 0$, with $0.1l_0$ radius in the domain shown in Fig. 3. All velocities in the internal grid points are set to zero. The wall temperatures are set to 112 °C ($T^* = 1$) as in the experiments of Kandlikar et al. [13]. The vapor

inside the bubble is set to saturation temperature of 100 °C ($T^* = 0$). The liquid temperature inside the domain is set equal to the inlet liquid temperature. All physical properties are taken at 100 °C. The inlet liquid temperature T_{in} is set to 103 °C. The contact angle at the walls is specified as 40° which is obtained from the experimental data of Balasubramanian and Kandlikar [1].

4.7. Boundary conditions

The boundary conditions are as following

At the outlet ($x^* = 3.96$):

$$u_x = v_x = w_x = T_x = 0; \; \phi_x = 0 \quad (15)$$

At the plane of symmetry ($z^* = 0$):

$$u_z = v_z = w = T_z = 0; \; \phi_z = 0 \quad (16)$$

At the walls ($y^* = 0$, $y^* = 0.99$):

$$u = v = w = 0; \; T = T_w; \; \phi_y = -\cos\varphi \quad (17)$$

where ϕ is the contact angle

At the wall ($z^* = 0.495$):

$$u = v = w = 0; \; T = T_w; \; \phi_z = -\cos\varphi \quad (18)$$

At the inlet ($x^* = 0$):

$$u = 1; \; v = w = 0; \; T = T_{in}; \; \phi_x = -\cos\varphi \quad (19)$$

Numerical calculations are done with three different area ratios between the two ends of the microchannel. The restricted end is always at $x^* = 0$. Three different area ratios are studied which are $R = 1$, 0.5 and 0.04. The area ratio R is defined as the ratio between the cross-section areas at $x^* = 0$ and at $x^* = 3.96$.

The mass flux at the channel inlet for all the cases is kept fixed at 20 kg/m² s. As the channel cross-section is restricted, the inlet velocity is increased to maintain the same mass flux.

5. Experiments

Figs. 4 and 5 show the experimental results obtained by Kandlikar et al. [13] for flow boiling in parallel microchannels with restricted inlets. The liquid mass flux G is equal to 120 kg/m² s and the wall heat flux q'' is equal to 298 kW/m². Thus, the average mass flux through each channel is 20 kg/m² s.

In Fig. 4, frames from (a) to (e) are taken at 1.17 ms time interval. The pressure drop element at the channel inlets has 51% open area. Normal flow reversal is observed in a single channel from a set of six parallel horizontal microchannels. The wall temperature in this case is $T_w = 112.4$ °C.

In Fig. 5, successive frames are shown from (a) to (f) taken also at 1.17 ms time intervals. The pressure drop element at the channel inlets has 4% open area. Stabilized flow is observed in a single channel from a set of six parallel horizontal microchannels. The wall temperature in this case is $T_w = 111.5$ °C.

6. Numerical results

The numerical calculations start with the bubble nucleating at $x = 0.2$ mm for the different area ratios. Since the length of the channel is 0.8 mm, the bubble is initially at one-third distance from
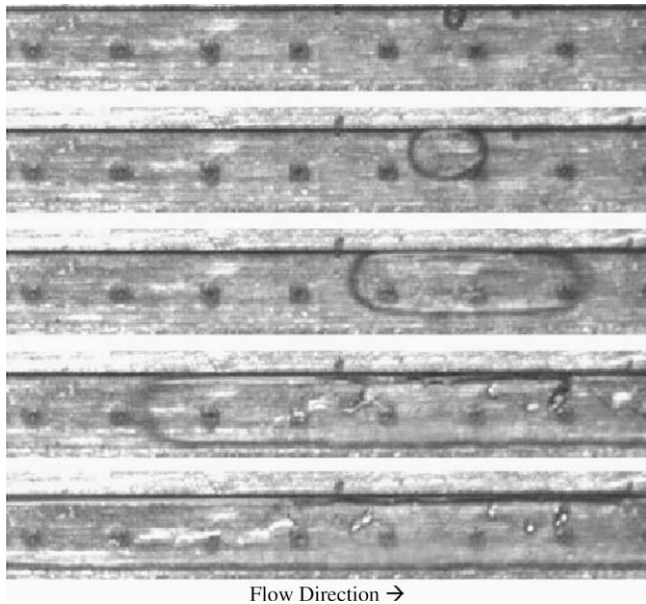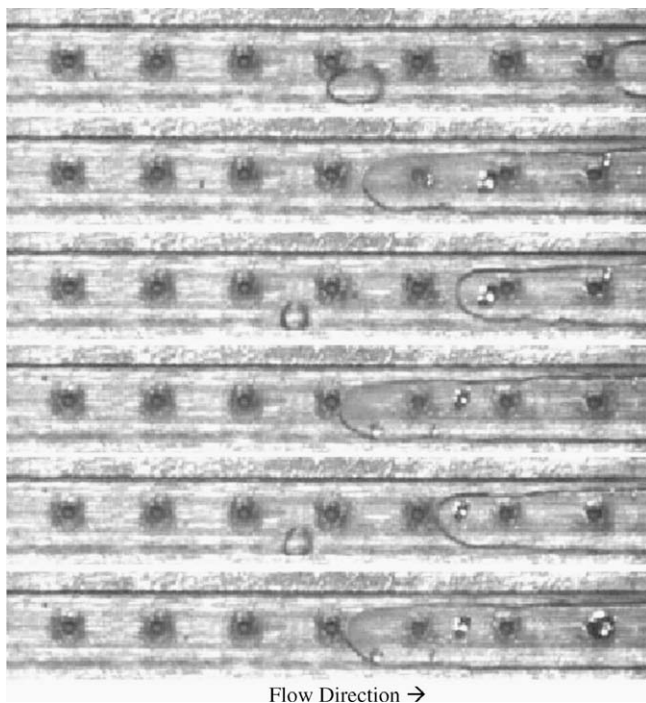
Fig. 4. Unstable flow with 51% area pressure drop elements and fabricated nucleation sites, successive frames taken at 1.17 ms time interval.

the channel outlet as compared to the channel inlet. The bubble grows in time due to evaporation at its interface. Initially the shape of the bubble is spherical. However, as the bubble grows big enough to almost fill the channel cross-section, it starts to elongate along the channel axis.

Fig. 6 shows the bubble shapes for $R = 1.0$. The time corresponding to each frame is indicated on the top right corner of each frame in milliseconds. The bubble grows in both positive and negative x directions at the downstream and upstream ends, respectively. At 0.11 ms the bubble has grown big enough to reach the channel outlet at $x^* = 4$.

Fig. 5. Stable flow with 4% area pressure drop elements and fabricated nucleation sites, successive frames taken at 1.17 ms time interval.

Figs. 7 and 8 show the bubble shapes for $R = 0.5$ and $R = 0.04$, respectively. In these cases inlet velocities are higher compared to $R = 1.0$ to maintain a constant mass flux. The bubble growth is suppressed due to higher liquid velocities around the bubbles. In case of $R = 0.04$, the bubble size at the end of 0.11 ms is the smallest. The downstream end of the bubble has only reached three-fourths of the channel length in this case whereas in the same duration the bubbles reached the channel end in the other two cases (Figs. 6 and 7).

Fig. 9 plots the bubble equivalent diameters against time for different values of area ratios R. The equivalent diameter is defined as the diameter of a sphere of equal volume as the bubble. As the area
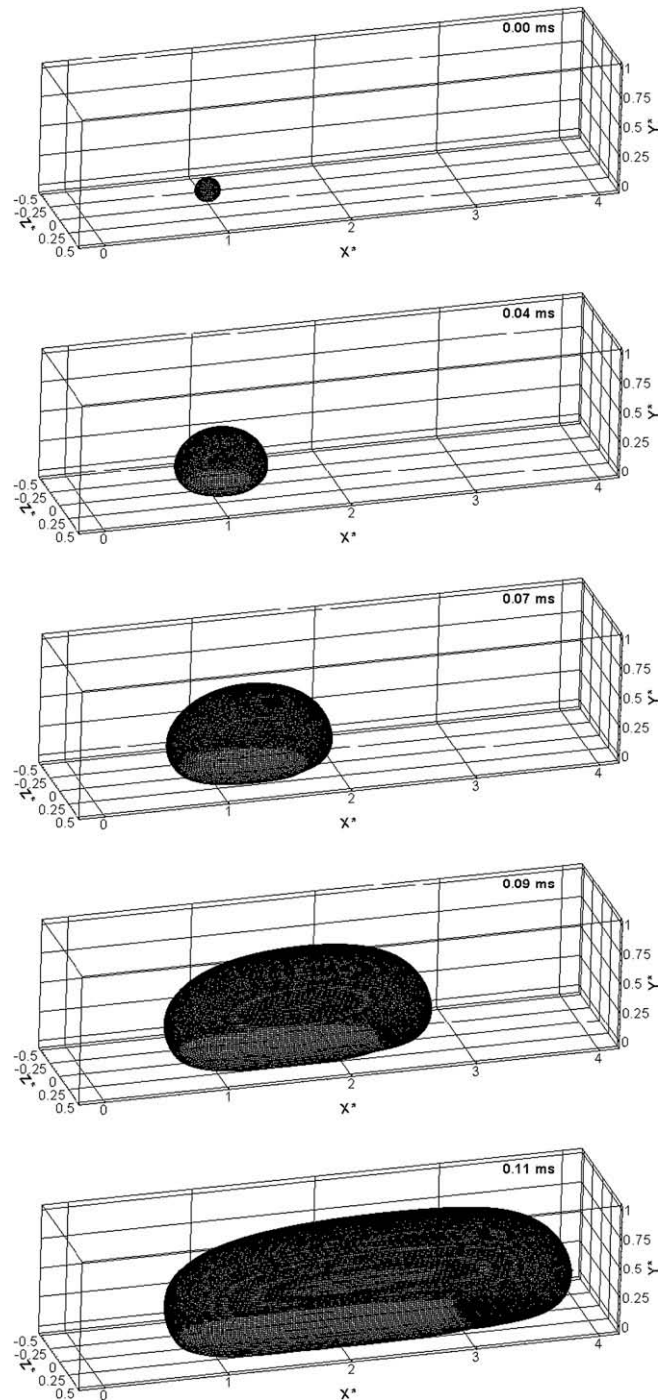

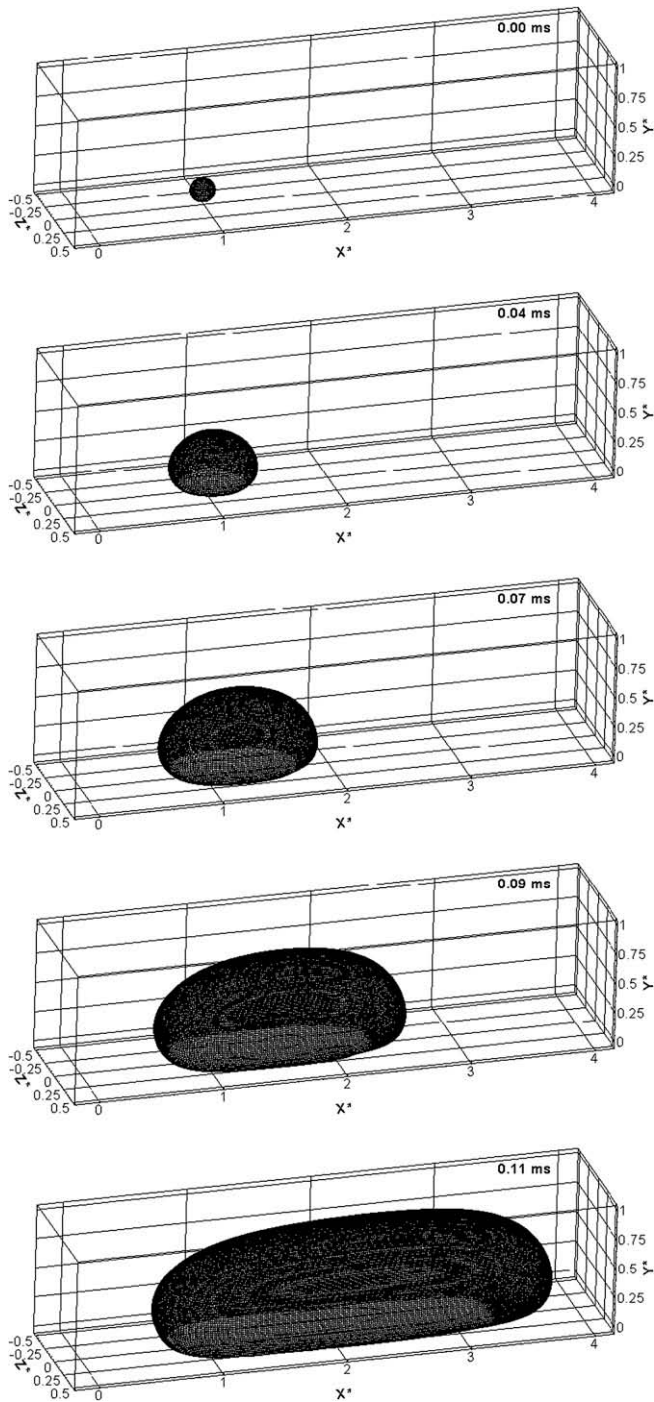**Fig. 6.** Numerically calculated bubble shapes for $R = 1.0$.

Fig. 7. Numerically calculated bubble shapes for $R = 0.5$.
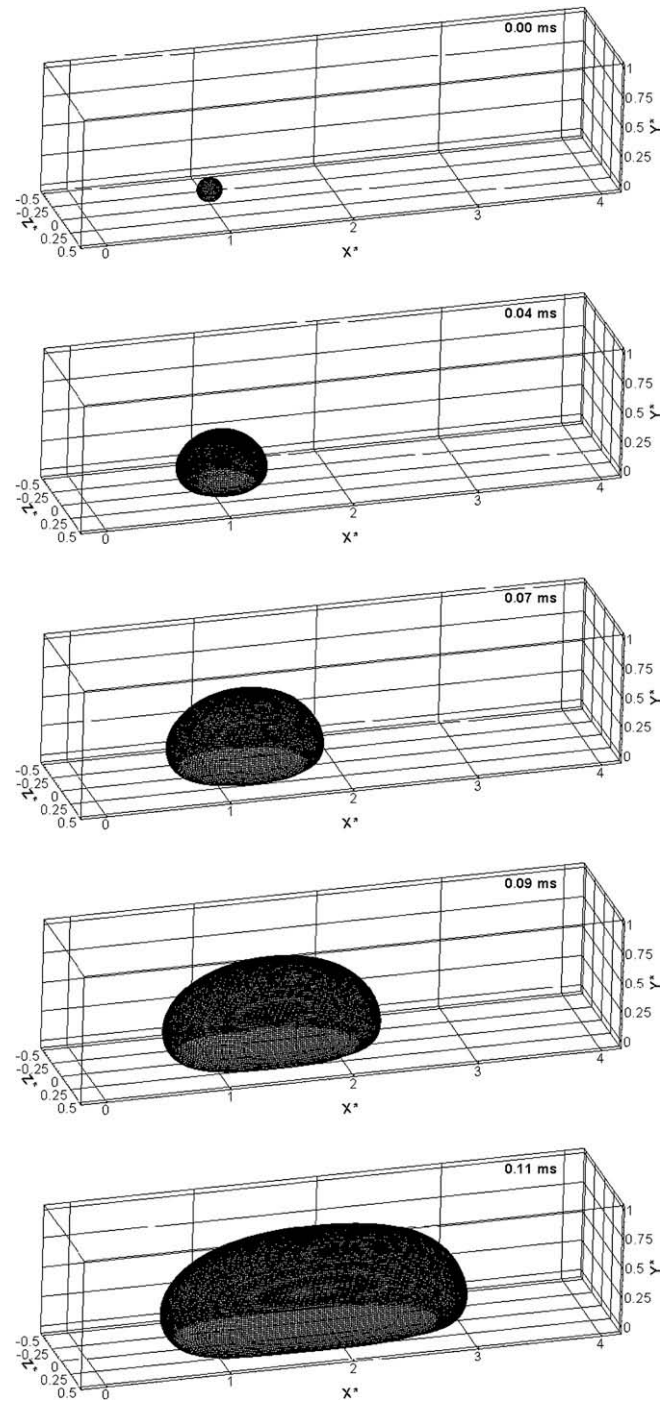

Fig. 8. Numerically calculated bubble shapes for $R = 0.04$.

ratio decreases, the bubble growth slows down due to the higher incoming liquid velocities. There are small differences in the bubble growth rates for $R = 1.0$ and $R = 0.5$. However, for $R = 0.04$, the bubble grows much slower compared to the other two cases. This conforms to the experimental results presented in Figs. 3 and 4. In the experiments, reversed flow was present in case of $R = 0.5$ but stabilized flow was observed for $R = 0.04$. In case of the numerical results, the bubble growth rate is found to be little affected at $R = 0.5$ as seen in Fig. 7. However, when $R = 0.04$, the bubble growth rate is much less and the movement of the bubble upstream end towards the channel inlet is limited, indicating stabilized unidirectional flow boiling.

Fig. 10(a)–(c) compares the velocity vectors around the bubbles for different values of R. The time is 0.07 ms for all the cases after initiation of calculations. The figures show the velocity vectors at the central x–y plane through the bubble and at the channel inlet. The reference vector is shown in each frame. In all cases, the velocity vectors on the left hand side are much longer than those on the right hand side of the bubble, indicating that liquid is flowing out of the domain in the positive x direction. It can be clearly seen that with a decrease in R, the magnitude of the velocity vectors at the downstream of the bubble get smaller indicating slower bubble growth rates. The bubble downstream interface velocities in the three cases at 0.07 ms are calculated as 1.14 m/s, 1.1 m/s and 0.27 m/s for R
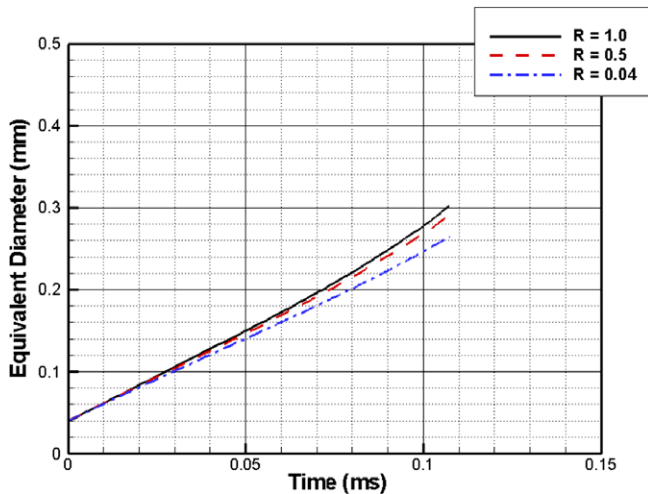
Fig. 9. Comparison of bubble growth for different area restriction ratios.

values of 1, 0.5 and 0.04, respectively. The magnitude of the velocity vectors at the channel inlet is seen to get larger with decrease in R, due to higher inlet velocities. The slower bubble growth rate is preventing a rapid pressure rise inside the channel that could be responsible for reversed flow towards the channel inlet.

Fig. 11(a)–(c) compares the thermal fields for different values of R at time 0.09 ms. The figures show temperature contours at the central x–y plane through the bubble. Contours are plotted for non-dimensional temperature between 0 and 1 at intervals of 0.2. Velocity vectors of uniform size have also been shown in each frame. The effect of channel restriction on the inlet velocity profile is clearly visible as the liquid enters the channel through a smaller opening. It can be seen that the bubble size decreases with R. This is due to the fact that the inertia of the liquid is preventing the bubble growth towards the upstream end of the channel. But since the liquid mass flux is the same in all cases, the area restriction has no significant impact on the growth of the thermal boundary layer at the channel walls. The higher inlet velocity near the channel centerline is getting obstructed by the bubble nucleating at the channel wall. A high pressure zone is created near the bubble upstream interface preventing the bubble growth in the reversed direction. The obstructed liquid tries to flow around the bubble through the liquid layer between the bubble and the channel walls, thus locally preventing growth of thermal boundary layer at the walls. The thickness of the liquid layer between the top of the bubble and the channel wall in the three cases are 42, 44 and 58 μm, respectively. A local increase in liquid velocity is causing the wall heat transfer to be in the form of sensible heat suppressing the thin film evaporation around the bubbles. The explosive bubble growth is thus contained which in turn prevented reversed flow inside the microchannel.

7. Discussion

The vapor bubble dynamics inside the microchannel is influenced by the geometry of the channel as well as by the rapid growth rate. As seen from Figs. 6–8, the vapor bubble initially grows in nearly spherical shape but gradually transforms to a plug under the influence of the enclosing channel walls. It is also seen that the bubble grows more towards the channel outlet without restriction.

The instability during flow boiling inside microchannels, as observed by several researchers, is caused primarily by the rapid growth and reversed vapor flow into the inlet manifolds. When a vapor bubble turns into a plug, the length of the plug increases
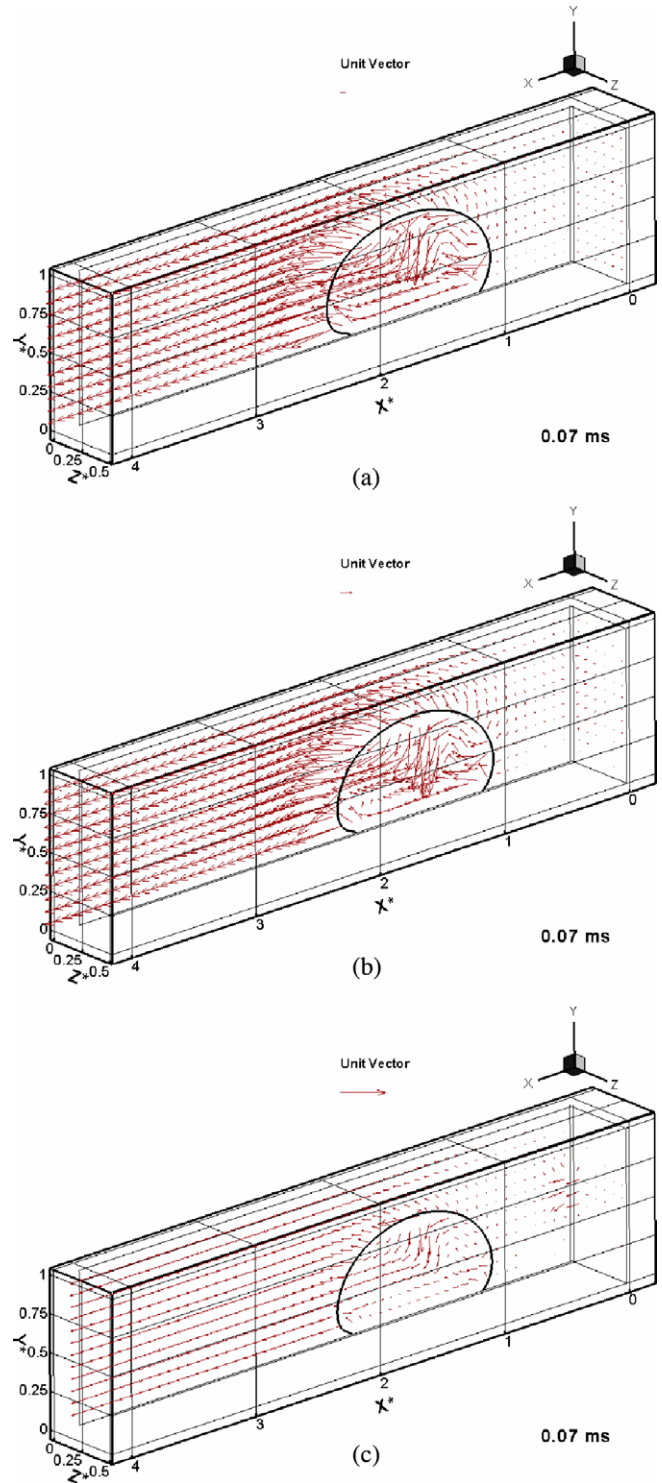

Fig. 10. Comparison of velocity fields for different area restriction ratios: (a) $R = 1$, (b) $R = 0.5$ and (c) $R = 0.04$.

with time. The end interfaces of the vapor plug have been observed to accelerate along the channel axis with interface velocities reaching as high as 3.5 m/s [1].

It has been shown by Mukherjee and Kandlikar [15] that a vapor plug traps a thin layer of liquid between its interface and the channel walls that lead to high vapor generation rate. However, the shape of the vapor plug itself can be a reason that causes the ends of the vapor plug to accelerate, increasing the pressure inside the channel. The following calculations will illustrate the point.
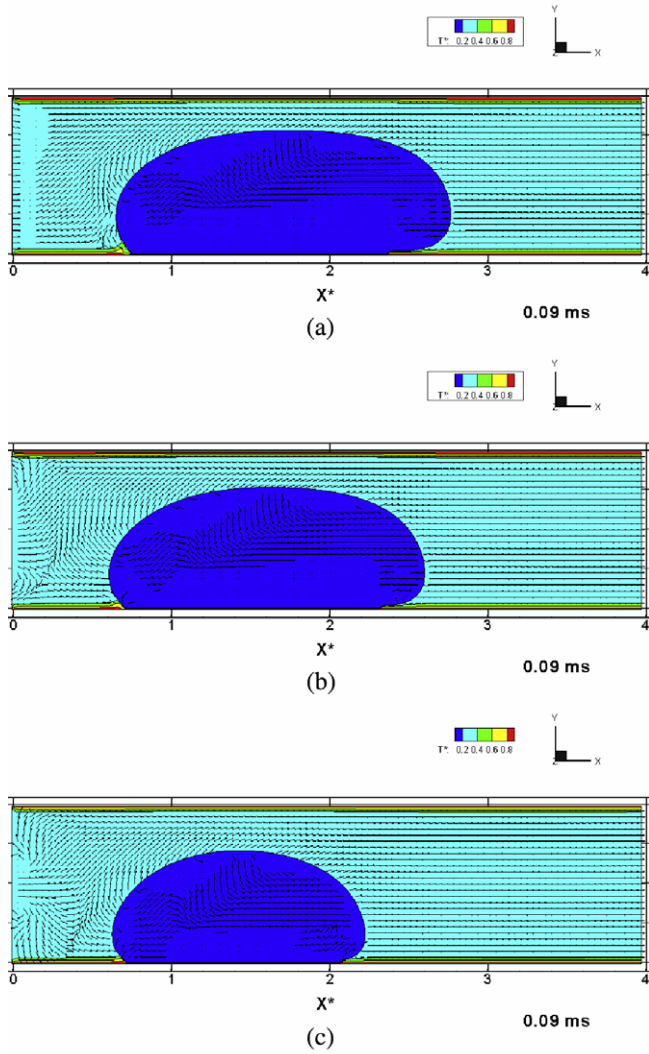
Fig. 11. Comparison of temperature fields for different area restriction ratios: (a) $R = 1$, (b) $R = 0.5$ and (c) $R = 0.04$.

Fig. 12(a) shows a spherical vapor bubble of diameter D growing in a sea of superheated liquid. The addition of mass to the bubble per unit time is given by

$$\pi D^2 \vec{m} = \rho_v \frac{dV}{dt} = \rho_v \frac{d}{dt}\left(\frac{\pi}{6}D^3\right) = \frac{\pi}{2}\rho_v D^2 \frac{dD}{dt} \tag{20}$$

Therefore, the rate of change in bubble diameter is given by

$$\frac{dD}{dt} = \frac{2\vec{m}}{\rho_v} \tag{21}$$

In case of a cylindrical bubble (Fig. 12(b)) of fixed diameter D but variable length L, the rate of mass addition to the bubble (neglecting the hemispherical ends for simplicity, since $L \gg D$) is given by

$$\pi D L \vec{m} = \rho_v \frac{dV}{dt} = \rho_v \frac{d}{dt}\left(\frac{\pi}{4}D^2 L\right) = \frac{\pi}{4}\rho_v D^2 \frac{dL}{dt} \tag{22}$$

Thus the rate of change of plug length is given by

$$\frac{dL}{dt} = \frac{4L\vec{m}}{D\rho_v} \tag{23}$$

The above calculations assume constant vapor density.

Thus, for a spherical bubble, the rate of change of bubble diameter is independent of the bubble diameter, whereas in the case of a cylindrical bubble enclosed by walls, the rate of increase in
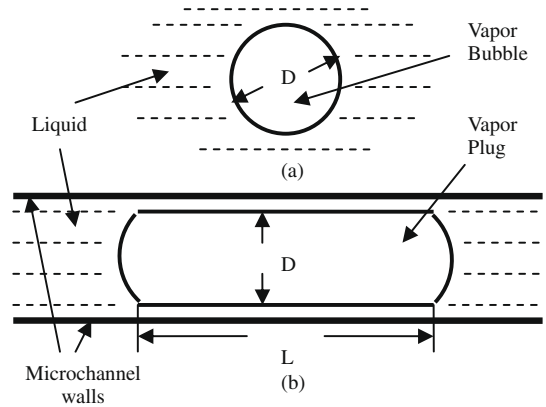

Fig. 12. (a) Spherical bubble in a pool of liquid. (b) Cylindrical bubble inside a microchannel.

bubble length is proportional to the length of the bubble. Thus, when the bubble shape changes from spherical to cylindrical inside a microchannel, its end velocities increase with the bubble length. This causes the plug interfaces along the channel axis to accelerate thereby increasing the pressure inside the channel.

It may be noted here that if the elongated vapor plug eventually touches the surrounding walls forming vapor patches, the vapor addition to the bubble will decrease thereby decreasing the plug interface velocity. However, this leads to deterioration in heat transfer and possible initiation of a CHF condition.

7.1. Proposed channel shapes

The reversed flow in the microchannels occurs mainly due to pressure build up inside the channel as a result of rapid vapor bubble growth. In order to have a unidirectional flow inside the channels, it is necessary to prevent the vapor plug acceleration and relieve the build up pressure inside the channels in the direction of the desired flow. It is proposed that microchannels be designed with increasing area ratio in the desired direction of flow thereby allowing the vapor plugs to grow with a constant interface velocity. This is possible if the cross-sectional area of the channel increases with the length of the channel.

Mukherjee and Kandlikar [20] have showed that with no inflow of liquid, a vapor bubble growing inside a microchannel restricted at one end grows predominantly towards the unrestricted end. The effect of the incoming liquid will further reduce the bubble growth and stabilize the flow as seen in the present study.

Mukherjee and Kandlikar [20] proposed diverging microchannel shapes that will ensure stable unidirectional flow without excessive
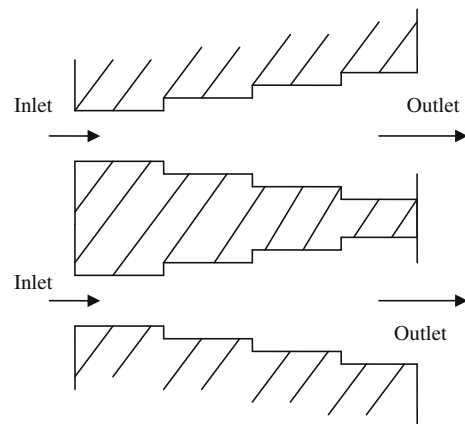

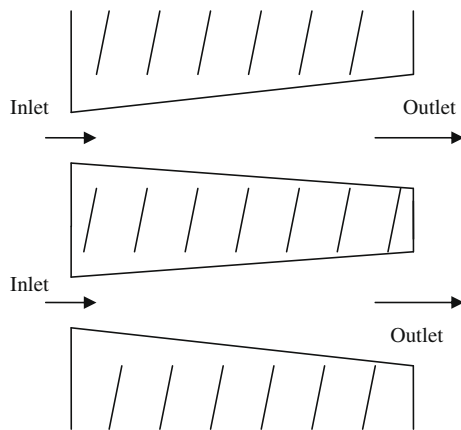**Fig. 13.** Conceptual stepped parallel microchannels.

Fig. 14. Conceptual diverging parallel microchannels.

pressure drops. Fig. 13 shows top view of conceptual microchannels with stepped walls that will progressively provide increasing area in the direction of flow. It will also help in preventing back flow of liquid from each individual section of the channel with constant cross-sectional area, due to the presence of restriction at its upstream end. The number and length of each section should be chosen carefully such that the thin film evaporation around the bubbles in each section can be sustained without dry out.

If manufacturing stepped microchannels pose a challenge, smooth diverging microchannels (shown in Fig. 14) may be used instead, to essentially provide the same benefits as the stepped channels. Again, the diverging angle should be chosen so as not to reduce the overall heat transfer in the microchannels.

Recently, Lu and Pan [21] experimentally studied flow boiling in diverging microchannels. Ten parallel microchannels with a diverging angle of 0.5° was used in the study. The results confirmed that diverging microchannels can result in more stable flow compared to channels with uniform cross-section.

8. Conclusions

The growth of a vapor bubble inside a microchannel during flow boiling is numerically studied with restrictions placed at the channel inlet. The choice of inlet restrictions have been made from previously obtained experimental data. The bubble growth rate is found to decrease significantly with 4% open area at the channel inlet which is consistent with the experimental results. The restriction at the channel inlet resulted in higher inlet velocities. The incoming high speed liquid gets obstructed by the nucleating bubble resulting in a zone of high pressure at the upstream end of the bubble. The obstructed liquid tries to flow through the liquid layer between the bubble and the channel walls thereby reducing thin film evaporation and restricting bubble growth. The results show that to be effective, the area ratio has to be quite small resulting in increased pressure drop. To prevent flow instabilities and pressure rise inside the microchannel due to accelerating vapor plugs,

it is suggested that microchannels be designed with increasing area ratio in the direction of desired flow.

References

[1] P. Balasubramanian, S.G. Kandlikar, Experimental study of flow patterns, pressure drop and flow instabilities in parallel rectangular minichannels, in: Proceedings of the Second International Conference on Microchannels and Minichannels 2004, Rochester, NY, 2004, pp. 475–481, ICMM2004-2371.
[2] G. Hetsroni, A. Mosyak, Z. Segal, G. Ziskind, A uniform temperature heat sink for cooling of electronic devices, Int. J. Heat Mass Transfer 45 (2002) 3275–3286.
[3] Y. Peles, Two-phase boiling flow in microchannels—instabilities issues and flow regime mapping, in: Proceedings of the First International Conference on Microchannels and Minichannels 2003, Rochester, NY, 2003, pp. 559–566, ICMM2003-1069.
[4] H.Y. Wu, P. Cheng, Boiling instability in parallel silicon microchannels at different heat flux, Int. J. Heat Mass Transfer 47 (2004) 3631–3641.
[5] J. Li, P. Cheng, Bubble cavitation in a microchannel, Int. J. Heat Mass Transfer 47 (2003) 2689–2698.
[6] H.Y. Wu, P. Cheng, Visualization and measurements of periodic boiling in silicon microchannels, Int. J. Heat Mass Transfer 46 (2003) 2603–2614.
[7] J. Li, G.P. Peterson, Boiling nucleation and two-phase flow patterns in forced liquid flow in microchannels, Int. J. Heat Mass Transfer 48 (2005) 4797–4810.
[8] K.H. Chang, C. Pan, Two-phase flow instability for boiling in a microchannel heat sink, Int. J. Heat Mass Transfer 50 (2007) 2078–2088.
[9] G. Wang, P. Cheng, H. Wu, Unstable and stable flow boiling in parallel microchannels and in a single microchannel, Int. J. Heat Mass Transfer 50 (2007) 4297–4310.
[10] G. Wang, P. Cheng, A.E. Bergles, Effects of inlet/outlet configurations on flow boiling instability in parallel microchannels, Int. J. Heat Mass Transfer 51 (2008) 2267–2281.
[11] S.G. Kandlikar, M.E. Steinke, S. Tian, L.A. Campbell, High-speed photographic observation of flow boiling of water in parallel mini-channels, in: Proceedings of NHTC'01, in: 35th National Heat Transfer Conference, Anaheim, CA, 2001, NHTC01-11262.
[12] M.E. Steinke, S.G. Kandlikar, Flow boiling and pressure drop in parallel flow microchannels, in: Proceedings of the First International Conference on Microchannels and Minichannels, Rochester, NY, 2003, pp. 567–579, ICMM2003-1070.
[13] S.G. Kandlikar, W.K. Kuan, D.A. Willistein, J. Borrelli, Stabilization of flow boiling in microchannels using pressure drop elements and fabricated nucleation sites, J. Heat Transfer 128 (2006) 389–396.
[14] H. Yuan, H.N. Oguz, A. Prosperetti, Growth and collapse of a vapor bubble in a small tube, Int. J. Heat Mass Transfer 42 (1999) 3643–3657.
[15] A. Mukherjee, S.G. Kandlikar, Numerical simulation of growth of a vapor bubble during flow boiling of water in a microchannel, J. Microfluidics Nanofluidics 1 (2) (2005) 137–145.
[16] S.V. Patankar, Numerical Heat Transfer and Fluid Flow, Hemisphere Publishing Company, Washington, DC, 1980.
[17] S.V. Patankar, A calculation procedure for two-dimensional elliptic situations, Numer. Heat Transfer 4 (1981) 409–425.
[18] M. Sussman, P. Smereka, S. Osher, A level set approach for computing solutions to incompressible two-phase flow, J. Comput. Phys. 114 (1994) 146–159.
[19] R.P. Fedkiw, T. Aslam, B. Merriman, S. Osher, A Non-Oscillatory Eulerian Approach to Interfaces in Multimaterial Flows (The Ghost Fluid Method), Department of Mathematics, UCLA, CAM Report 98-17, Los Angeles, 1998.
[20] A. Mukherjee, S.G. Kandlikar, Numerical study of the effect of inlet constriction on bubble growth during flow boiling in microchannels, in: Proceedings of ICMM05, Third International Conference on Microchannels and Minichannels, Toronto, Canada, 2005, ICMM2005-75143.
[21] C.T. Lu, C. Pan, Stabilization of flow boiling in microchannel heat sinks with a diverging cross-section design, J. Micromech. Microeng. 18 (7) (2008) 4896. Art. No. 075035.